Composites: Part A 173 (2023) 107635

Contents lists available at ScienceDirect

Composites Part A

journal homepage: www.elsevier.com/locate/compositesa

Inter-ply friction behaviour in the temperature assisted forming of magnesium/glass fibre reinforced thermoplastic polymer laminates

Zheng Liu, Enrico Simonetto, Andrea Ghiotti, Stefania Bruschi *

Department of Industrial Engineering, University of Padova, Via Venezia 1, 35131 Padova, Italy

ARTICLE INFO

Keywords:
Magnesium alloy-based fibre metal laminates (FMLs)
Thermoplastic prepregs
Inter-ply friction
Surface roughness

ABSTRACT

The paper investigates the metal/prepreg inter-ply friction behaviour in thermoplastic fibre metal laminates (FMLs) based on magnesium alloy and glass fibre-reinforced polymer (GFRP) under a range of parameters (normal pressure, relative sliding velocity, temperature) that are typical of forming processes conducted at elevated temperature on FMLs. The surface roughness of metal sheets was also varied and its influence on the inter-ply friction behaviour was evaluated. Pull-through tests with a stop-start controlling strategy were designed and carried out for identifying the inter-ply friction coefficient at varying conditions. To support the quantitative data from the tests microscopic observations were performed on the residues of the prepregs left on the tested metal sheets. The obtained results proved that the differences in the friction coefficient are strongly dependent on the process conditions and the metal surface roughness. The increase in the relative sliding displacement enables the transition from the hydrodynamic to the mixed lubrication mode according to the Stribeck theory, which further rises the friction coefficient. The inter-ply friction coefficient is observed to increase at decreasing temperature and normal pressure, and at increasing sliding velocity and metal surface roughness.

1. Introduction

The ever-increasing request of the transportation industry for a reduction of fuel consumption and therefore CO_2 emissions is pushing more and more the use of structural materials with a high strength-to-weight ratio. Fibre metal laminates (FMLs) as a form of hybrid laminated material system, made up of thin metal sheets laminated with fibre-reinforced polymer layers (FRPs, also called prepregs in the following), can answer this demand. The combination of metals and FRPs can take advantage of both the material types, namely FMLs can overcome the reduced toughness of FRPs and enhance the mechanical resistance of monolithic metal sheets at the same time [1–3]. FMLs, such as glass-reinforced aluminium laminates (GLARE), aramid-reinforced aluminium laminates (ARALL), and carbon-reinforced aluminium laminates (CARALL), have been introduced in the aerospace sector to reduce the overall weight and improve the impact and fatigue responses of aerospace structural parts [4–6]. However, since the last decade, there has been an interest in new materials as FML constituents. As regards the metal sheets, driven by the increasing demand for high strength-to-density parts, magnesium alloy- and titanium alloy-based FMLs are becoming more and more attractive. Even though the impact resistance [7] and most static properties [8–9] of magnesium-based FMLs are lower than the aluminium-based ones currently employed in actual constructions, they show high potential in primary aerospace structures subjected to compression buckling, and some secondary structures, for example, the leading edges, for the purpose of weight saving [10]. Additionally, effective electromagnetic interference shielding enables the widening of their application as well [11–12]. For the polymer matrix of the composite core, thermoplastic materials have been recently introduced for recyclability issues, allowing carrying out forming processes at elevated temperature to shape the components.

Thermoforming is indeed a suitable strategy to manufacture FMLs parts of industrial interest, as it provides high production efficiency, but with reduced overall manufacturing costs at the same time. Nevertheless, this forming procedure becomes particularly challenging when fabricating complex-shaped components, such as those characterized by double curvatures. The deformation mechanisms taking place during forming at elevated temperatures include intra-ply and inter-ply shearing, out-plane bending, tension, and compression [13–14]. In particular, inter-ply friction is relevant to the sliding between two adjacent plies (both prepreg/prepreg and metal/prepreg). The layers being formed to a curved shape can induce the onset of wrinkling defects

* Corresponding author.
E-mail address: Stefania.Bruschi@unipd.it (S. Bruschi).

https://doi.org/10.1016/j.compositesa.2023.107635
Received 17 February 2023; Received in revised form 15 May 2023; Accepted 27 May 2023
Available online 31 May 2023

if the generated compressive strain cannot be alleviated by inter-ply sliding [15]. Moreover, inter-ply friction can induce undesired changes in the yarns, which, in turn, can lead to fibre in-plane undulations or waviness in the formed part [16]. The analysis of the inter-ply friction behaviour is then mandatory to fulfil a proper design of the process assuring high-quality components.

Pull-out [17–18] and pull-through [19–20] tests are usually employed to characterize the inter-ply friction behaviour: during these tests, the inner ply of the laminate is drawn from the outer plies with a compressive normal pressure applied on the overlapping area of the stacked structures. In the pull-out tests, the contact area between the prepreg and metal layers decreases at increasing pulling distance since the metal sheet inserted between the prepregs only protrudes at one end during the test. While in the pull-through tests, the contact area can be kept constant by keeping the metal sheet extruding at both ends of the contact area, such that a uniform pressure distribution can be assured during the test. Using a standardized procedure, Sachs et al. [21] compared various friction test setups in terms of measured coefficients of friction between Twintex®PP and mild steel sheets. A pronounced difference in the kinetic friction coefficients from pull-through and pull-out tests was found under the same experimental parameters due to the inhomogeneous pressure distribution being likely to develop during the pull-out tests. Actually, during the forming process of FMLs, no voids between the outer plies should occur since the migration of the inner plies away from one region would draw materials from other places into this region [22]. Consequently, the contact area is recommended to be kept constant, as is in the pull-through tests, which, therefore, better represent the actual forming process.

Due to the polymer matrix being greatly influenced by the forming conditions, the major challenge in characterizing the inter-ply friction is to figure out how much the inter-ply response is resin-dominated (hydrodynamic regime) or fibre-dominated (boundary regime). Compared to the inter-ply friction behaviour of a dry fabric that is dominated by the Coulomb friction, the addition of the polymer matrix brings complexity to the system being the polymer viscosity strongly sensitive to the process parameter variations. During the thermoforming process carried out on FMLs, the polymer matrix between the metal sheets and fabric layer is in a liquid state, so that it can be treated as a liquid lubricant film between the adjacent layers. Accordingly, the Stribeck theory, depicting the inter-ply friction throughout all the lubrication ranges [23], can be employed to assess the influence of the process parameters on the inter-ply friction. Fig. 1 shows the Stribeck curve, which reports the kinetic friction coefficient as a function of the Hersey number (H), the latter being dependent on the viscosity (η) of the lubricant, relative sliding velocity (v), and normal pressure (p) (see Eq. (1)).

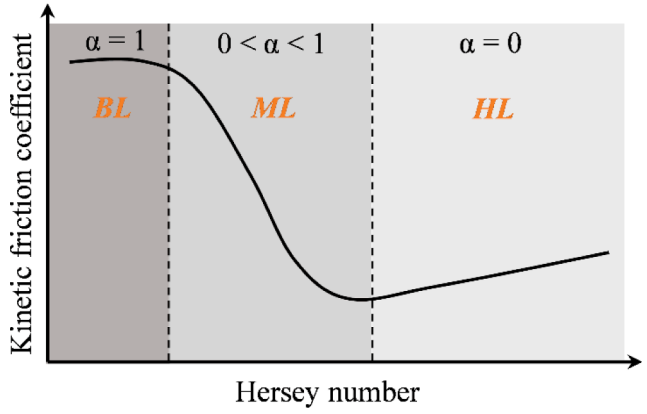

Fig. 1. Schematic of the Stribeck curve. (For interpretation of the references to colour in this figure legend, the reader is referred to the web version of this article.)

$$H = \frac{\eta v}{p} \tag{1}$$

The graph area can be divided into three zones according to the different types of contact between the adjacent layers. When the metal sheets and fabric are totally separated by the liquid polymer, hydrodynamic lubrication (HL) occurs. In this case, the shear stress (τ) is given by Eq. (2), where h is the thickness of the lubricant film.

$$\tau = \frac{\eta v}{h} \tag{2}$$

If no liquid polymer separates the adjacent layers, boundary lubrication (BL) occurs, characterized by a Coulomb-type response. When both of the above-mentioned lubrication modes are found at the same time, namely the inter-ply friction is contributed partly by the polymer matrix and partly by the fabric layer, mixed lubrication (ML) takes place. When addressing the mixed case for FMLs, the Coulomb and hydrodynamic friction mechanisms exist simultaneously. To model the shear stress in such conditions, Chow [24] proposed Eq. (3).

$$\tau = \frac{\mu_c N_c + \eta \frac{v}{h} A_r}{A_T} \tag{3}$$

where μ_c is the Coulomb friction coefficient at the metal-fibre interface, Nc the normal load pertaining to the Coulomb friction, Ar the contact area between the metal sheets and the molten polymer matrix, and A_T the total contact area between the metal sheets and prepregs. Finally, the effective friction coefficient (μ_{eff}) is given by Eq. (4), where α between 0 and 1 indicates how much the boundary lubrication governed by the Coulomb friction is present compared to the hydrodynamic one.

$$\mu_{eff} = \alpha\mu_c + (1-\alpha)\frac{\eta v}{hp} \tag{4}$$

By substituting Eq. (1) into Eq. (4), Eq. (5) is obtained:

$$\mu_{eff} = \alpha\mu_c + (1-\alpha)\frac{H}{h} \tag{5}$$

Therefore, α discriminates the type of inter-ply friction. When $\alpha = 1$, the fibre-dominated inter-ply friction is governed by the Coulomb friction coefficient μ_c, which means that the boundary lubrication regime applies exhibiting a solid-solid contact. The inter-ply friction presents a liquid matrix-dominated characteristic within the hydrodynamic lubrication range when $\alpha = 0$, and the boundary condition pertains to a solid-liquid contact. When $0 < \alpha < 1$, the inter-ply friction is located in the mixed lubrication regime.

Numerous researchers have investigated how process parameters such as the normal pressure, sliding velocity, and temperature affect the inter-ply friction behaviour within the hydrodynamic lubrication area [25–26]. Chow [24] performed experiments to analyse the inter-ply friction of commingled glass polypropylene four-harness satin-weave fabric between the binder ring and the die. The obtained results of the above-mentioned research were located in the transition area of the Stribeck curves, identifying a mixed and hydrodynamic lubrication behaviour. Rashidi et al. [27] tested the inter-ply friction behaviour between two layers of epoxy-based prepregs with plain weave structures where the decrease in the coefficient of friction was observed at increasing normal force, which was demonstrated to be within the mixed lubrication regime. Furthermore, the inter-ply friction in this regime was modelled by employing an inverse hydrodynamic-lubrication (IHL) theory and an asperity contact model [28]. Besides the process parameters mentioned above, the fibre orientation was also experimentally proved to significantly influence the friction coefficients at the metal/prepreg interface of epoxy-based GLARE sheets [29].

Moreover, when a fluid film is established between two adjacent layers, the friction mostly depends on the shearing of the polymer matrix at the interface [30]. Due to the mobility and flow characteristics of the epoxy matrix at elevated temperatures, its thickness dynamically varies

not only at varying process parameters [27], but also at varying relative sliding of the plies of the composite core over each other [28]. This leads to the so-called dynamic response of the inter-ply friction, which is exhibited by the increased shear stress as the shear strain rises after the yield point of the shear stress.

For the composite core, CFRPs with thermoset polymers as matrix have been widely applied [31–32]. Nevertheless, since thermoplastic polymers guarantee reduced cycle time, recyclability, and better compatibility with current stamping lines [33], they are becoming an alternative to thermoset ones as matrices of the composite core and have attracted a great deal of interest from academic and industrial researchers. However, thermoplastic polymers have a significantly lower melt viscosity than thermosetting ones [9], bringing various issues during the forming process that may affect the final performances of the formed components, including impregnation of fibres, and the presence of voids during the consolidation process of the matrix during forming [34]. From the viewpoint of tribology, the higher mobility and flow characteristic of thermoplastic polymers at elevated temperatures brings a higher sensitivity of the inter-ply friction to different processing parameters.

Delamination, as a main defect in the service life of FML components, highly affects their mechanical performances [35]. It occurs when the metal/matrix interfacial bonding strength is not strong enough at different loading conditions as well as thermal cycles [36–37]. Therefore, before the fabrication of the FML components, various pretreatments are usually carried out on the FMLs to enhance the interfacial bonding strength between the metal and prepreg surfaces; which have been proven to reduce delamination defects [38–39] and improve impact [40] and fatigue [41] resistances of the formed components. The addition of nanofillers such as carbon nanotubes (CNTs) in the polymer matrix has proved to be a valid strategy to enhance the metal/matrix adhesively bonding strength [42]. The effective pretreatments performed on the metal surfaces include mechanical techniques, such as grit/sand-blasting [43–44], chemical methods like anodizing [45] and etching [46–47], and the addition of interfacial layers through plasma spray [48]. The surface treatment modifies the texture and morphology of the metal sheet surfaces, further altering the boundary conditions between the metal and prepreg. In particular, the surface roughness has been proved to primarily influence the friction coefficient, as was studied in [49] between a pin and a disc with oil lubrication throughout a range of Hersey numbers. The variation in the metal sheet surface roughness introduces another potential factor influencing the inter-ply friction behaviour of FMLs. While most of the current investigations on the inter-ply friction behaviour of FMLs when formed at elevated temperature concern the effect of the forming parameters and fibres orientation, no literature records are available dealing with the influence of the metal sheet surface roughness on the inter-ply friction behaviour of FMLs.

In this framework, the objective of the paper is to provide a comprehensive understanding of the inter-ply friction mechanisms when forming magnesium-based FMLs at elevated temperature with a thermoplastic matrix. The dynamic response of the inter-ply friction to the relative sliding displacement is evaluated under various process parameters, namely the normal pressure, sliding velocity, and temperature, and the sensitivity of inter-ply friction to the metal sheet surface roughness is evaluated as well. Section 2 of the paper reports the characteristics of the investigated FMLs, the qualification of the metal sheets after surface conditioning, and the description of the employed experimental procedures. Section 3 describes the test results at varying process parameters, including the effect of metal sheet surface roughness on the inter-ply friction under various process parameters. Finally, Section 4 summarizes the main conclusions.

2. Material and methods

2.1. Material

The FMLs investigated in this study consist of AZ31B magnesium alloy sheets (thickness of 0.5 mm) and Tepex® 102-RG600 (2)/47% Type B prepregs (thickness of 1 mm), which are stacked together as described in section 2.3. Table 1 reports the main characteristics of the prepregs. The prepregs consist of Polyamide 6 (PA6) matrix and glass fibres with a Twill 2/2 weaving style. The mechanical properties of the magnesium alloy sheets and the ones of the prepregs in the as-received condition, shown in Table 2, were assessed by performing standard tensile tests (ISO-6892) on a 50 kN MTS™ 322 hydraulic dynamometer.

2.2. AZ31B surface pre-treatments

The surface of the metal sheets was properly conditioned with the aim of enhancing the interfacial bonding strength between them and the prepreg layer, which, in turn, improves the in-service performances of the formed component. In addition, the quality of the metal surface, mainly in terms of roughness and texture, is recognized to significantly affect the inter-ply friction behaviour. Sandblasting, as an efficient, low-cost, and environmentally friendly method has been widely applied in industry to mechanically modify the topography of the surface of large-scale metal components. A subsequent annealing treatment can bring an extra enhancement to the interfacial bonding strength by exploiting the surface chemical oxidation when magnesium alloy sheets are considered [50]. In view of this, the combination of sandblasting and annealing was selected for surface conditioning in this study. To achieve varying metal surface roughness, the surfaces of the AZ31B sheets were first sandblasted (*S*) using white corundum with a grain size of F80 at different pressures. Then, the sandblasted sheets were annealed (*SA*) by holding them at 500 °C for 20 min in a furnace, followed by air cooling at room temperature, after which three levels of surface roughness (*Sa*) were achieved, namely 1.55 ± 0.1, 2.28 ± 0.12, and 2.63 ± 0.17 μm. To make the description as simple as possible, the nomenclature of Sa_L, Sa_M, and Sa_H was chosen to indicate the three surface roughness levels, namely the subscript *L* means low, *M* medium, and *H* high roughness. Fig. 2 shows the surface topographies of the untreated (UT) and treated AZ31B sheets. The marked orientation induced by the rolling process, as is evident in the UT case in Fig. 2 (a), was eliminated by the surface treatment and replaced with the relatively isotropic surface textures shown in Fig. 2 (b), (c), and (d).

2.3. Stop-start pull-through tests

The testing device shown in Fig. 3 (a) and (b) was designed and realized in accordance with the ASTM standard D3528 [51], which is used to assess the tensile and shear strengths of adhesives used in metal bonding. This testing device makes use of a doubly lapped specimen to determine the metal/prepreg inter-ply friction coefficient. Two horizontal layers of prepreg and one vertical layer of metal sheet placed between the former ones were used to fabricate the cross-shaped

Table 1
Prepregs characteristics.

Layup	Value
Matrix	PA6
Melting point (matrix)	220 °C
Fibre	E-Glass
Weaving style	Twill 2/2
Area weight (dry fabric)	600 g/m^2
Yarn count	1200 tex
Weight rate	50 %
Fibre content	47 %
Laminate density	1.8 g/cm^3

Table 2
Mechanical properties of the AZ31B sheets and prepregs.

AZ31B sheet	Value	Prepreg	Value
Elastic Modulus	45 GPa	Tensile modulus	18 GPa
Yield Strength	158 ± 2 MPa	Ultimate Tensile strength	380 ± 5 MPa
Ultimate Tensile Strength	248 ± 4 MPa	Strain at break	2.3 %
Shear Modulus	16.7 GPa	Flexural Modulus	16 GPa
Poisson's Ratio	0.35	Flexural Strength	300 ± 5 MPa

specimen whose sketch and dimensions are given in Fig. 4. The samples were tested in a plate-plate configuration with a constant overlapping area of 20 × 20 mm^2. They were heated in an MTS™ 651 environmental chamber to the designed temperature before being tested on the MTS™ 322 hydraulic dynamometer. The metal sheet was pulled through the two prepregs with the normal pressure exerted by the compression spring shown in Fig. 3 (a). Various normal pressures were applied by regulating the stroke of the compression spring. The metal sheet was gripped on the lower clamp so that the pulling velocity was controlled and the pulling force was monitored in the meanwhile. Before assembling the specimen, the testing set-up was preheated to the designed temperature for 1 h to ensure an even temperature distribution and avoid the difference in the temperature between the set-up and specimen. For the wet friction case, which is relevant to testing temperatures above the polymer matrix melting point, the entire stroke given to the magnesium alloy sheet in the pulling direction (that was 25 mm) was uniformly divided into 5 stages (hereafter S_{w1} to S_{w5}) as shown in the left part of Fig. 4 in order to evaluate the possible influence of the relative sliding displacement between the metal and the prepreg layers on the inter-ply friction. While, for the dry friction case, which is relevant to testing temperatures below the polymer matrix melting point, the inter-ply friction is more sensitive to the relative sliding displacement, therefore more stages (hereafter S_{d1} to S_{d6}) were considered in the first 10 mm displacement as shown in the right part of Fig. 4. The inter-ply friction coefficient at each stage was obtained by employing a stop-start control strategy. Within one stage, the pulling of the AZ31B sheet

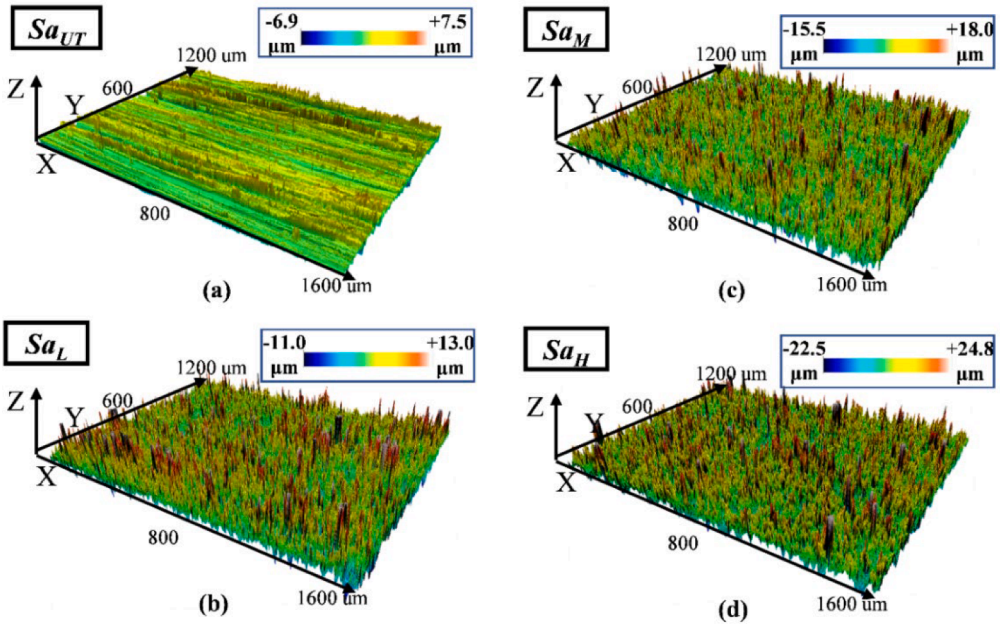

Fig. 2. Surface topographies of the AZ31B sheet samples for (a) untreated, (b) low surface roughness (c), medium surface roughness, and (d) high surface roughness. (For interpretation of the references to colour in this figure legend, the reader is referred to the web version of this article.)

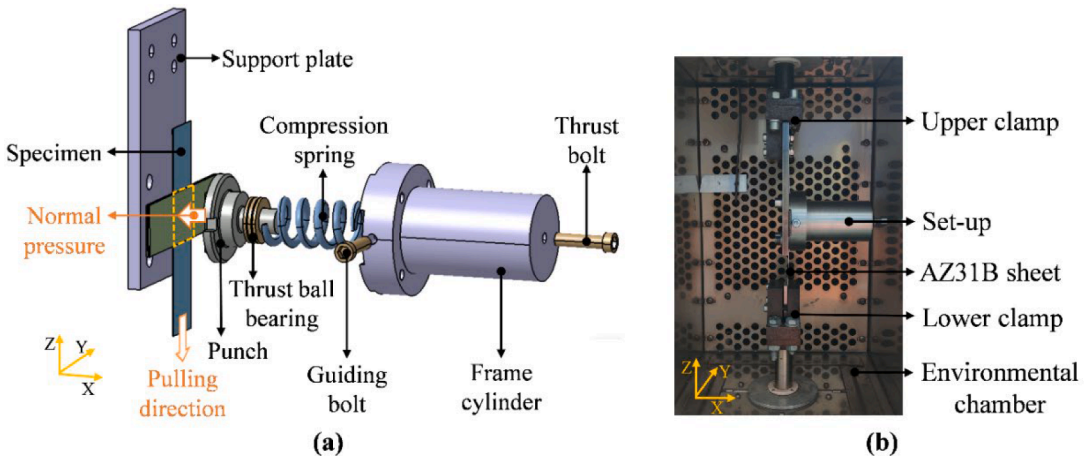

Fig. 3. Stop-start pull-through test: (a) scheme, and (b) assembly. (For interpretation of the references to colour in this figure legend, the reader is referred to the web version of this article.)

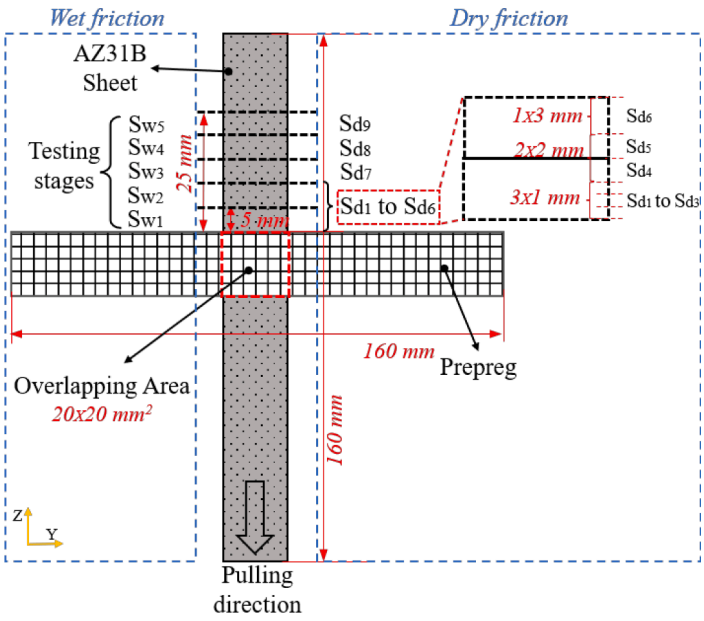

Fig. 4. Sketch and dimensions of the specimen used in the stop-start pull-through tests. (For interpretation of the references to colour in this figure legend, the reader is referred to the web version of this article.)

was controlled in a distance-control mode, allowing the test to be performed at a specific velocity while the pulling force as a function of relative sliding displacement was tracked in real time. Each stage of the test ended with a one-minute break to relax and relieve the shear stress before the following stage began.

Pull-through experiments with AZ31B sheets having variable surface roughness under various loading conditions were carried out. Table 3 reports the testing parameters selected in this study. It is worth noting that the testing temperatures of 235 °C and 255 °C were selected to analyse the inter-ply friction behaviour above the melting temperature of the polymer matrix of the prepreg PA6, which is 220 °C. On the contrary, the testing temperature of 215 °C was chosen to compare the possible differences in the inter-ply friction behaviour above and below the melting temperature of the polymer matrix. The PA6 viscosity at the temperatures of 235 °C and 255 °C was calculated using the Carreau model as shown in Fig. 5 with the coefficients reported in [52]. To ensure the reproducibility of the results, five tests were repeated for each testing condition.

2.4. Analysis of the tested samples

To progressively analyse whether the inter-ply friction is dominated by the resin or fibres of the FML composite core, their residues on the AZ31B magnesium sheets after the pull-through tests were microscopically examined. Firstly, the tested AZ31B sheets were cleaned with an ultrasonic acetone bath for 10 min followed by a rinsing process in demineralized water, after which the specimens were dried by compressed air. Then, the FEI QUANTA 450™ Scanning Electron Microscope (SEM) equipped with a backscattered Electron Detector (BSED) was employed to assess the residues of the prepreg core on the surfaces of the tested AZ31B sheets at each stage.

Table 3
Pull-through testing parameters.

Parameter	Baseline	Values	Unit
Normal pressure p	2.5	0.5, 2.5, 5	MPa
Velocity v	0.5	0.1, 0.5, 1	mm/s
Temperature T	235	215, 235, 255	°C
Metal surface roughness Sa	Sa_M	Sa_L, Sa_M. Sa_H	

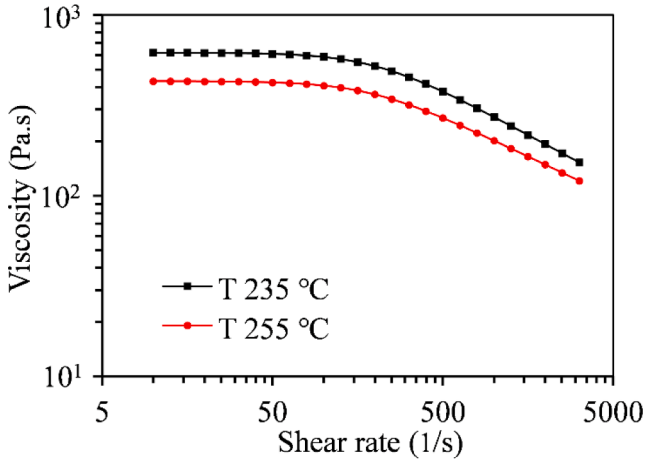

Fig. 5. PA6 viscosity at temperatures of 235 °C and 255 °C. (For interpretation of the references to colour in this figure legend, the reader is referred to the web version of this article.)

3. Results and discussion

3.1. Influence of the relative sliding displacement

Besides the flow characteristics of the polymer matrix in the liquid state as mentioned in § 1, the geometrical architecture of the prepreg is another factor influencing the dynamic response of the inter-ply friction to the relative sliding displacement, which can be easily understood through the sketches illustrated in Fig. 6. The 3D structure of the FMLs is shown in Fig. 6 (a). The inter-ply friction shows a dynamically varying response as the contacting surfaces change. When the inter-ply friction is relevant to the metal/polymer matrix interface as in Fig. 6 (b), it falls into the hydrodynamic lubrication range, while, as the thickness of the polymer matrix layer gradually reduces, it enters the mixed lubrication range when the metal surface comes in contact with the fibres as shown in Fig. 6 (c).

Fig. 7 presents the evolution of the inter-ply shear stress and friction coefficient at different stages with the processing parameters fixed at the

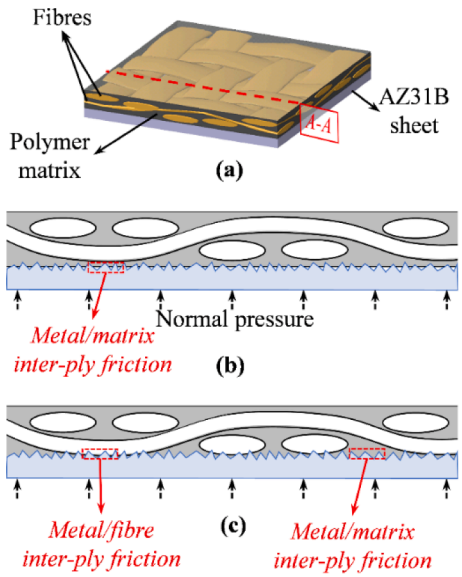

Fig. 6. 3D view of the contact between the metal sheet and prepreg (a); possible contact between the metal sheet and the prepreg at cross-section A-A: metal-polymer matrix (b); metal-polymer matrix & fibres (c). (For interpretation of the references to colour in this figure legend, the reader is referred to the web version of this article.)

baseline reported in Table 3. In Fig. 7 (b), the static (μ_s) and kinetic friction coefficients (μ_k) were obtained by Eq. (6) and Eq. (7) respectively, where τ_s and τ_k represent the static and kinetic shear stresses, obtained from the shear stress curve at the peak point and steady state, respectively.

$$\mu_s = \frac{\tau_s}{p} \tag{6}$$

$$\mu_k = \frac{\tau_k}{p} \tag{7}$$

Fig. 7 (a) clearly shows the different response of the shear stress as the stage increases. Firstly, a gradual increase in the shear stress can be observed as the stages rise. At S_{w1} and S_{w2}, the shear stress grows gradually until reaching a steady state, which suggests a liquid-like inter-ply shear feature and explains the limited gap between the static and dynamic friction coefficients at these stages (see Fig. 7 (b)). The morphology of the residues left on the surface of the tested magnesium alloy sheets shown in Fig. 8 provides further evidence of this phenomenon. At S_{w1}, the inter-ply shear occurred at the interface between the metal sheet and polymer matrix, as most of the residues found on the AZ31 sheets were indeed polymer matrix. The molten polymer matrix served as a liquid lubricant at the metal-prepreg interface throughout the first two stages. The metal sheet and prepreg were consequently separated by a liquid layer, indicating the hydrodynamic lubrication mode. Because of the higher relative sliding displacement from S_{w1} to S_{w2}, more molten polymer matrix was evacuated from the connecting area, resulting in a thinner polymer matrix layer. On the contrary, the presence of both the polymer matrix and the tangled fibres on the examined magnesium alloy sheets at S_{w3}, as depicted in Fig. 8 (b), reveals that the metal/prepreg inter-ply friction falls into the mixed lubrication range, as it is a combination of the metal/polymer matrix and metal/fibres inter-ply friction [24]. With the change in the lubrication mode, a new shear stress response arises, as seen in Fig. 7 (a), where the shear stress curve for S_{w3} drops after reaching the peak, evidently revealing a solid-like inter-ply shear response. The static and dynamic friction coefficients diverge more from S_{w3} to S_{w5} (Fig. 7 (b)). At S_{w5}, the difference between the two is maximum, which is further explained by the dominance of the mixture of fibres and polymer matrix

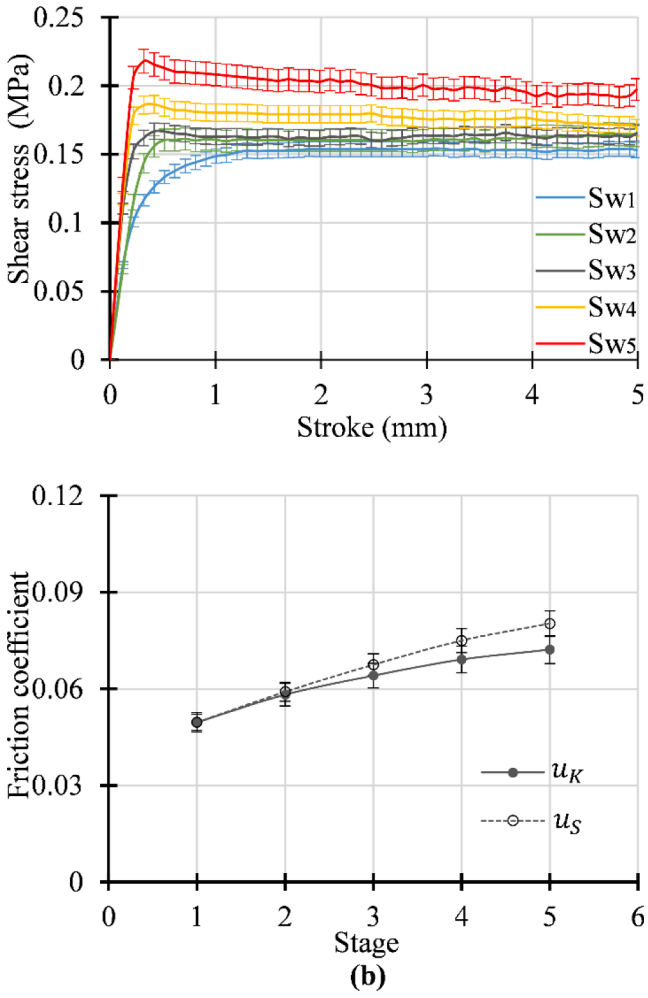

Fig. 7. Pull-through test results at different stages: (a) shear stress, and (b) friction coefficients. (For interpretation of the references to colour in this figure legend, the reader is referred to the web version of this article.)

residues on the tested AZ31 sheets as shown in Fig. 8 (c). Because the metal/fibre inter-ply friction coefficient (that is the Coulomb friction coefficient) is higher than the one at the metal/polymer matrix interface, the inter-ply friction coefficient also rises at increasing fibre volume fraction, which is the reason for the increase in both the inter-ply friction and shear stress from S_{w3} to S_{w5}. It is clear from S_{w1} to S_{w5} that the required stroke achieving the peak of the shear stress decreases as the stage rises, indicating the increase in the shear modulus of the system that is defined as the ratio of the peak shear stress to the corresponding shear strain. This can be explained by the increased viscosity of the interface layer at increasing fibre content [30].

According to the Stribeck theory, the normal pressure, relative sliding velocity, and resin viscosity all have a coupled effect on the inter-ply shear behaviour, changing the friction coefficient as the Hersey number does. The inter-ply friction in the hydrodynamic region is primarily affected by the molten resin changing behaviour as a result of the variation in the processing parameters. In the mixed lubrication zone, the percentage of Coulomb friction α in Eq. (5) is the most important factor in modifying the inter-ply friction.

As the polymer matrix shows varying thickness at varying processing conditions, a similar tendency can be seen in the inter-ply friction coefficient as a function of the relative sliding displacement at a given Hersey number (Fig. 9). In the hydrodynamic lubrication range where $\alpha = 0$, Eq. (5) can be simplified into Eq. (8), which indicates that the inter-ply friction coefficient is inversely proportional to the thickness of the

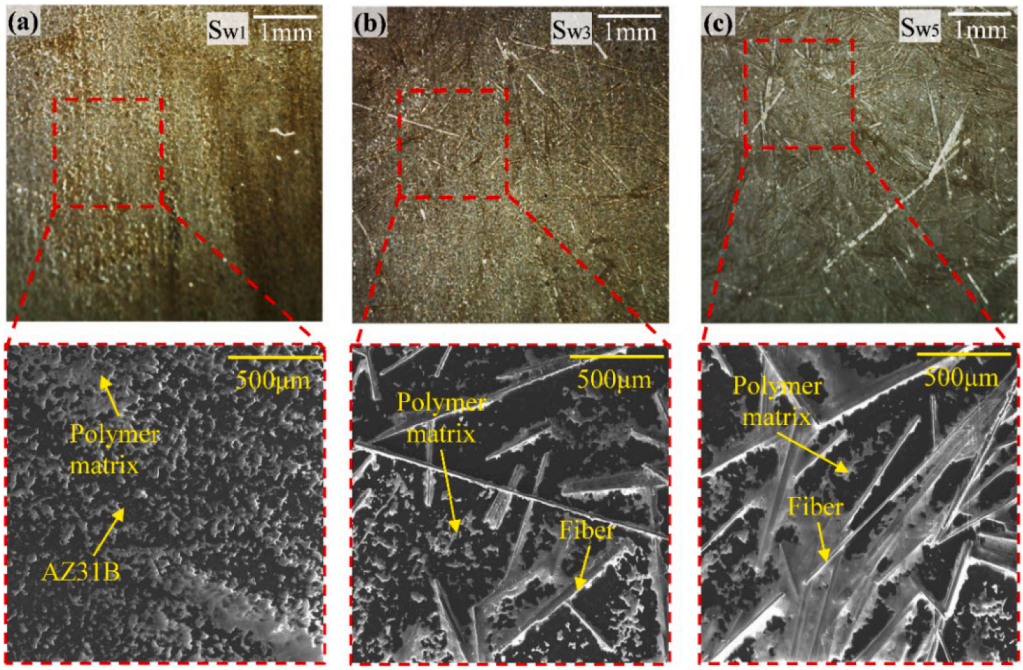

Fig. 8. Morphology of the residues on the tested magnesium alloy sheets after (a) stage 1, (b) stage 3, and (c) stage 5. (For interpretation of the references to colour in this figure legend, the reader is referred to the web version of this article.)

polymer matrix (h). Being h at S_{w1} higher than at S_{w2}, the friction coefficient raises from S_{w1} to S_{w2}.

$$\mu_{eff} = \frac{H}{h} \tag{8}$$

From S_{w3}, the mixed lubrication prevails, and by combining similar items with α in Eq. (5), Eq. (9) can be obtained.

$$\mu_{eff} = \left(\mu_c - \frac{H}{h}\right)\alpha + \frac{H}{h} \tag{9}$$

The effective inter-ply friction rises at increasing percentage of the Coulomb friction because the metal/fibres inter-ply Coulomb friction is higher than the one of the metal/polymer matrix hydrodynamic regime, which is consistent with the experimental results shown in Fig. 7. Accordingly, the inter-ply friction also exhibits a dynamic response to the relative sliding displacement at given Hersey number. Overall, this proves that the inter-ply friction is sensitive to the coupled effect of the processing parameters and relative sliding displacement.

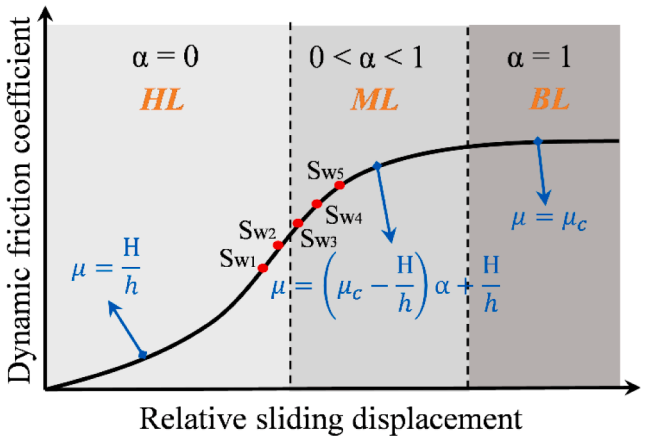

Fig. 9. Inter-ply dynamic friction coefficient at varying relative sliding displacement. (For interpretation of the references to colour in this figure legend, the reader is referred to the web version of this article.)

3.2. Influence of the normal pressure

In the thermoforming process of FML parts with curved shapes, having a normal pressure gradient is common due to the curved geometry character of the part and since different zones of the FLM touch the dies at different moments. Therefore, it is worth evaluating the influence of the normal pressure on the inter-ply shear behaviour at various stages. Fig. 10 illustrates the pull-through test results at varying normal pressure, being the other parameters fixed at baseline. As can be seen in Fig. 10 (a), the inter-ply shear stress (from $\tau^{P0.5}$ to τ^{P5}) increases across all the stages as the normal pressure increases from 0.5 MPa to 5 MPa. However, the inter-ply shear stress does not rise linearly at increasing normal pressure. At S_{w1}, when the pressure increases from 0.5 MPa to 2.5 MPa, the inter-ply friction (from $\mu^{P0.5}$ to $\mu^{P2.5}$) shows a liquid-like response and falls into the hydrodynamic lubrication regime, where a lower coefficient of friction can be found at increasing normal pressure, in agreement with the findings in [25]. This is because, at increasing normal pressure, the surface asperities of the fibre layer are flattened and its surface roughness decreases accordingly, which caused the drop of the inter-ply friction. The surface of the fibre layer is further flattened when the applied normal pressure is 5 MPa, but the friction coefficient rises as a result of the mixed lubrication mode brought on by the direct contact between the metal sheet and the fibre layer, as illustrated in Fig. 11(a). As a result, the inter-ply friction is higher at 5 MPa than at 2.5 MPa normal pressure. Additionally, different trends can be seen in the inter-ply shear stress as a function of the relative sliding displacement under various normal pressures. The testing result at 5 MPa normal pressure reveals a solid-like shear response at S_{w1}, while S_{w3} is identified as the point at which the response changes from being liquid-like to solid-like when the normal pressure is reduced to 2.5 MPa. The static and kinetic shear stresses between the metal and fibre layers are found to be different within the last two stages with a normal pressure of 0.5 MPa. The transition from a liquid-like inter-ply friction response to a solid-like one is hastened by the higher normal pressure. Since a higher amount of molten polymer matrix is squeezed out of the contacting area at a higher normal pressure before the test starts, the initial thickness of the polymer matrix between the metal and the fibre layers is reduced. Moreover, the higher shear stress brought by the

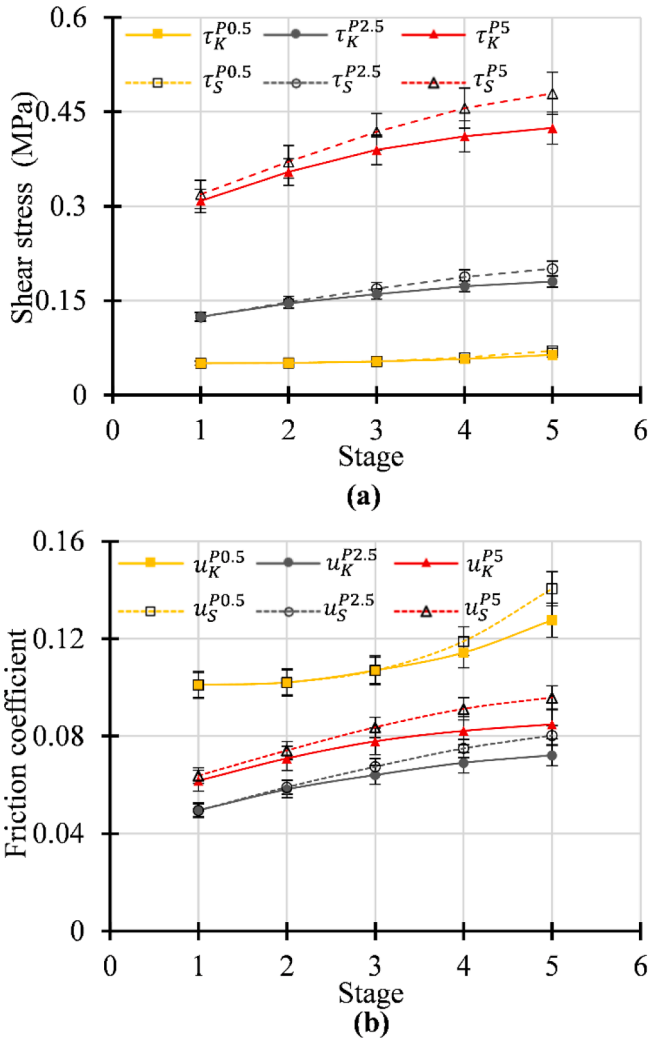

Fig. 10. Pull-through test results at varying normal pressure and different stages: (a) shear stress, and (b) friction coefficient. (For interpretation of the references to colour in this figure legend, the reader is referred to the web version of this article.)

higher normal pressure exacerbated the loss of resin as the relative sliding displacement rises. It is likely that this phenomenon facilitates the meeting between the metal and fibre layers. At the highest normal pressure, it is also found that the difference between the static and kinetic shear stresses widens along with the increased contact area between the metal and fibre layers.

3.3. Influence of the sliding velocity

Since the fibre layer moves through different parts of the set-up at different velocity even if the punch moves at a fixed velocity during the thermoforming process, it is also important to evaluate the inter-ply friction behaviour at varying sliding velocity. Fig. 12 shows the friction coefficients from the pull-through tests with the sliding velocity changing from 0.1 mm/s to 1 mm/s (from $\mu^{v0.1}$ to μ^{v1}), being the other parameters fixed at the baseline values.

It is evident that the higher the sliding velocity the higher the inter-ply friction through all the stages. At S_{w1}, the inter-ply friction coefficient increases as the relative sliding velocity rises. According to the power law of liquid viscosity (Eq. (10)), the inter-ply stress in the hydrodynamic lubrication range can be expressed through Eq. (11), where the m is the flow consistency index, $\dot{\gamma}$ the shear rate, and n the flow behaviour index. The shear thinning behaviour (parameter n to change from 0 to 1) of the molten PA6 matrix enables the shear stress to increase as the shear rate rises. As a result, as the sliding velocity rises, so does the friction coefficient in S_{w1}. What's more, the relative velocity also impacts the dynamic response of the inter-ply shear behaviour to the relative sliding displacement. The transition from a liquid-like response to a solid-like one is accelerated at increasing sliding velocity. The transition happens around S_{w5} at the sliding velocity of 0.1 mm/s, whereas it occurs at around S_{w2} when the speed is 1 mm/s. Furthermore, the gap between the static and kinetic friction coefficients in the mixed lubrication range becomes wider as the sliding velocity rises.

$$\eta = m(\dot{\gamma})^{n-1} \tag{10}$$

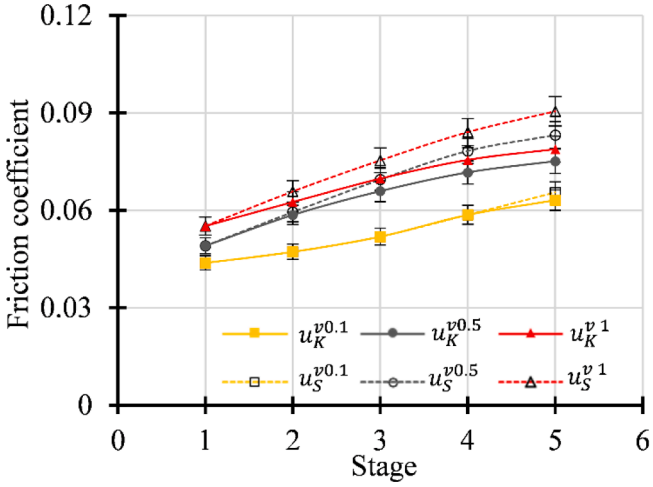

Fig. 12. Inter-ply friction coefficients at varying sliding velocity and different stages. (For interpretation of the references to colour in this figure legend, the reader is referred to the web version of this article.)

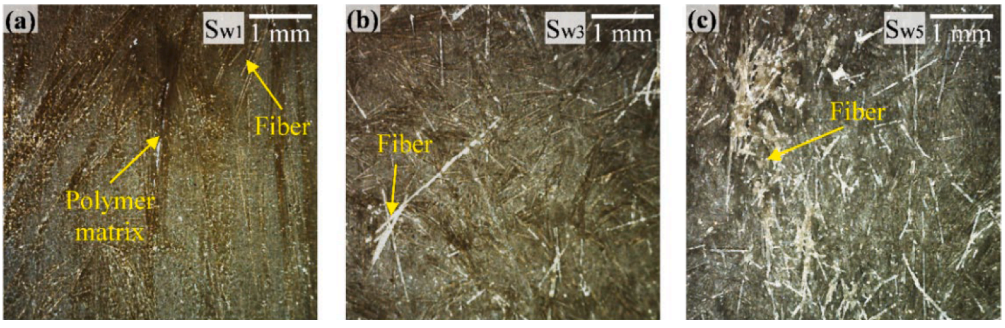

Fig. 11. Morphology of the residues on the tested magnesium alloy sheets at 5 MPa normal pressure after (a) stage 1, (b) stage 3, and (c) stage 5. (For interpretation of the references to colour in this figure legend, the reader is referred to the web version of this article.)

$$\tau = m(\dot{\gamma})^n \tag{11}$$

3.4. Influence of the temperature

The state and properties of the thermoplastic resin are highly sensitive to the forming temperature, further impacting the inter-ply friction behaviour. Inter-ply friction shows a dry response dominated by the Coulomb friction when the temperature is below the melting point of the thermoplastic polymer matrix. On the contrary, when the temperature is higher than its melting limit, the thermoplastic matrix exists in a liquid state acting as a lubricating film between the adjacent plies. Since the viscosity of the molten matrix is sensitive to temperature, the inter-ply friction is also temperature-dependent.

Fig. 13 shows the inter-ply friction at 235 °C (μ^{T235}) and 255 °C (μ^{T255}) at different stages with the processing parameters fixed at the baseline. As expected, at the highest temperature, a reduced viscosity contributes to decreasing the friction coefficient whatever the stage. Despite the fact that a larger inter-ply shear stress at a lower temperature should contribute to more polymer matrix being "washed away" from the contacting area and, therefore, the transition from the hydrodynamic to the mixed lubrication mode should be accelerated, the transition points at these two temperatures are both located at around S_{w2}. The temperature sensitivity of the prepreg can account for the observed phenomenon. The higher the temperature the more the molten polymer matrix that is squeezed out from the contacting region at a given normal pressure [53]. As a result, the polymer matrix layer becomes thinner at increasing temperature, which facilitates the contact between the metal and fibre layers.

To easily compare the effect of the temperature on the inter-ply friction behaviour at varying processing parameters, the Stribeck curve can be used to represent all the experimental data in a master curve. The exponential model displaying the relationship between the kinetic friction coefficient μ_K and the Hersey number H was chosen to fit the experimental data at varying stages as it was proven to suitably reproduce the inter-ply friction [29] (see Eq. (12), where A and B are the fitting parameters). The fitting parameters and the coefficient of correlation R^2 at each stage are reported in Table 4. Being all the R^2 values higher than 0.9, the exponential model provides a good fit for the experimental data. Fig. 14 (a) and (b) show the comparison between the experimental data (μ_K^{T235}– Exp & μ_K^{T255}– Exp) and the ones calculated using Eq. (12) (μ_K^{T235}– Fit & μ_K^{T255}– Fit) at temperature 235 °C and 255 °C respectively for the metal surface roughness Sa_M case. In Fig. 14 the coloured 3D surfaces are the fitting data, whereas the scatter plots are

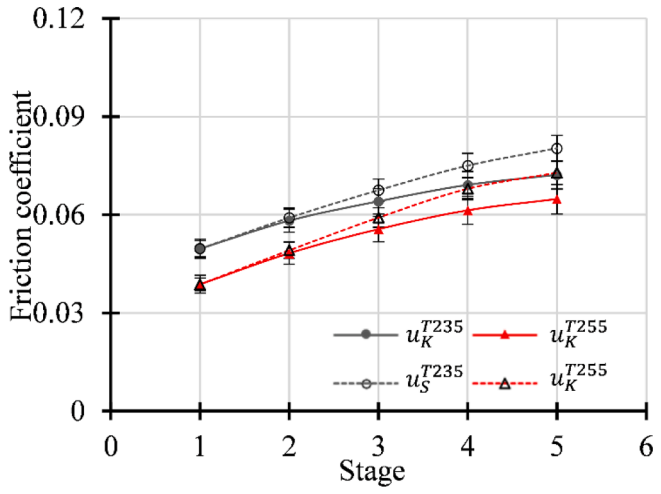

Fig. 13. Inter-ply friction coefficients at varying temperature and different stages. (For interpretation of the references to colour in this figure legend, the reader is referred to the web version of this article.)

the experiment results. As expected, a higher kinetic friction coefficient is found at 235 °C than at 255 °C regardless of the Hersey number and stage.

$$\mu_K = Ae^{BH} \tag{12}$$

The dry friction case was intended to not only provide insight into the Coulomb friction mechanisms at the interface between the metal and prepreg layers, but also to serve as a comparison for the above-mentioned results in case of molten polymer matrix presence. A typical inter-ply friction distribution at the temperature of 215 °C with all the other parameters fixed is shown by the grey curves ($\mu_K^{Sa_M}$) in Fig. 15. It can be observed that both the static and kinetic friction coefficients increase from S_{d1} to S_{d4}, with a subsequent steady state from S_{d5}. In contrast to the liquid-solid contact in the wet case, when the contact is solid-solid, the static friction coefficient is significantly higher than the kinetic one at all stages. At S_{d1}, due to the inter-ply friction occurring at the interface between the metal and unscratched matrix layers, the friction coefficient shows the lowest value. The surface of the polymer matrix becomes rougher (see the surface topography of the tested prepregs shown in Fig. 16 (a)) as the stages rise, leading to the increase in the inter-ply friction from S_{d1} to S_{d4}. The increasing tendency of the kinetic friction coefficient ends at S_{d5} and is followed by a stable level that is greater than the value before S_{d4} as a result of the additional inter-ply friction at the interface between the metal and fibre layers (see Fig. 16 (b)). This stable state clearly reveals that the inter-ply shear behaviour follows the Coulomb friction of a homogeneous material from S_{d5}. An explanation for this is that, in the dry friction case, the fabric is prevented from spreading by the solid polymer matrix, therefore the real contact area between the metal and fibre layers is confined to the peaks of the undulated yarns [27], as the broken fibres shown in Fig. 16 (b).

Fig. 15 also shows the inter-ply friction coefficient at varying metal surface roughness. As expected, the higher the metal surface roughness the higher the static (from $\mu_S^{Sa_L}$ to $\mu_S^{Sa_H}$) and kinetic (from $\mu_K^{Sa_L}$ to $\mu_K^{Sa_H}$) friction coefficients, indicating that both the metal/polymer and metal/fibre inter-ply frictions are sensitive to the metal surface roughness in case of dry condition.

3.5. Influence of the metal surface roughness

To explore the influence of the metal surface roughness on the inter-ply friction in case of molten polymer matrix, pull-through tests at 235 °C with magnesium sheets having different surface roughness were performed. The fitting parameters through the exponential model (Eq. (12)) of the kinetic friction coefficient at various metal surface roughness are listed in Table 5. Fig. 17 (a) and (b) show the comparison between the experimental data (from $\mu_K^{Sa_L}$- Exp to $\mu_K^{Sa_H}$- Exp) and the ones calculated using Eq. (12) results (from $\mu_K^{Sa_L}$- Fit to $\mu_K^{Sa_H}$- Fit) under the metal surface roughness Sa_H and Sa_L respectively, while the ones for Sa_M can be found in Fig. 14 (a). The higher the metal surface roughness the higher the kinetic inter-ply friction coefficient regardless of the Hersey number and stage. The D_{Sa} parameter calculated from Eq. (13) is here introduced to show the degree of the metal surface roughness influence on the variation in the kinetic friction coefficient at varying Hersey numbers and stages. The results reported in Fig. 18 show that the inter-

Table 4
Fitting parameters of Eq. (12) at varying temperature.

	T235°C			*T255*°C		
	A	**B**	**R^2**	**A**	**B**	**R^2**
S_{w1}	0.053	850.05	0.9139	0.039	1051.1	0.9045
S_{w2}	0.060	781.93	0.9121	0.045	963.31	0.9148
S_{w3}	0.066	754.92	0.9218	0.052	912.02	0.9116
S_{w4}	0.071	739.60	0.9405	0.058	876.00	0.9121
S_{w5}	0.075	751.87	0.9340	0.062	928.87	0.9332

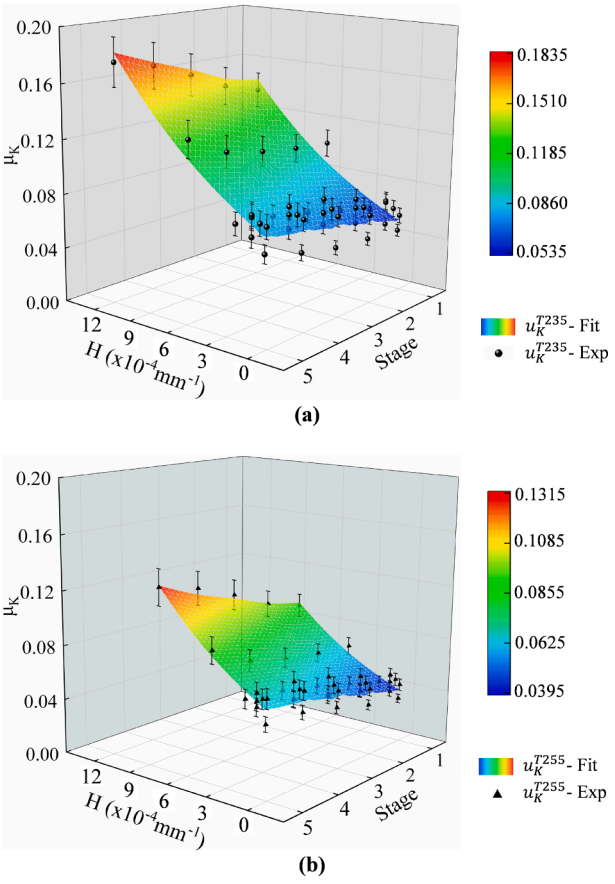

Fig. 14. Calculated and experimental kinetic inter-ply friction coefficients at varying Hersey number and stage at temperature (a) 235 °C (b) 255 °C under the metal surface roughness Sa_M. (For interpretation of the references to colour in this figure legend, the reader is referred to the web version of this article.)

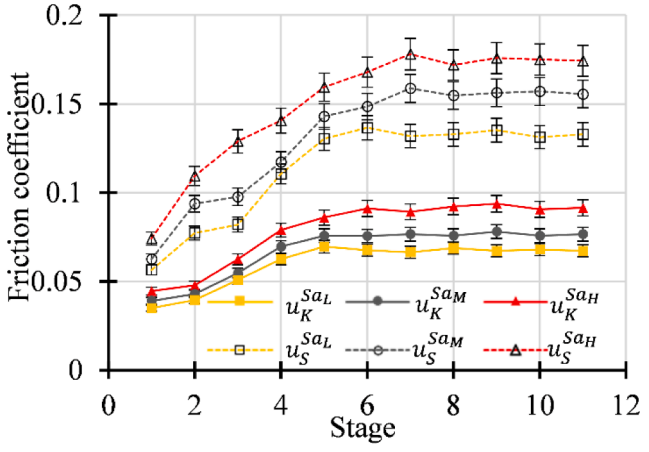

Fig. 15. Inter-ply friction coefficients at 215 °C at varying metal surface roughness and different stages. (For interpretation of the references to colour in this figure legend, the reader is referred to the web version of this article.)

ply friction is affected differently by the metal surface roughness in the various lubrication ranges. The black spots on the H-Stage plane are the projection of the test data located in the mixed lubrication range, which are used to make a distinction between the hydrodynamic lubrication range and the mixed one. The D_{Sa} parameter in the mixed lubrication range is higher than that in the hydrodynamic lubrication range, indicating that the metal/fibre inter-ply friction has higher sensitivity to the

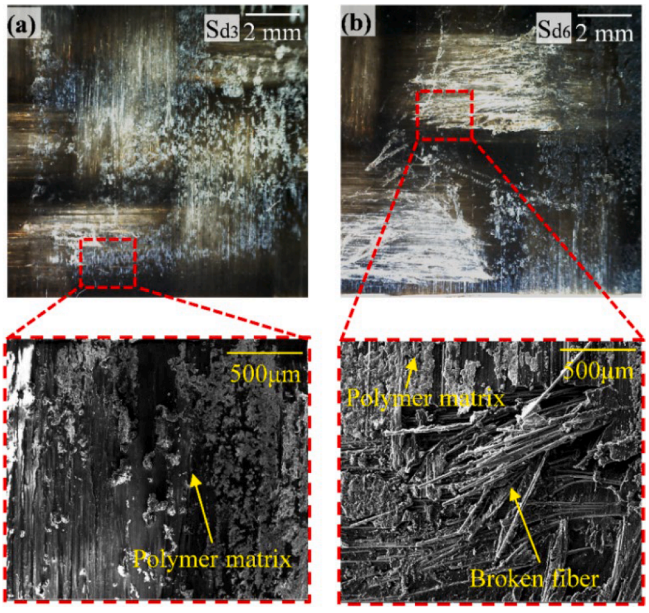

Fig. 16. Morphology of the residues on the tested magnesium alloy sheets with the metal surface roughness of Sa_M at 215 °C after (a) stage 3, and (b) stage 6. (For interpretation of the references to colour in this figure legend, the reader is referred to the web version of this article.)

metal surface roughness than the one when the molten polymer matrix is present at the interface.

$$D_{Sa} = \frac{\mu_k^{Sa_H} - \mu_k^{Sa_L}}{\mu_k^{Sa_L}} \tag{13}$$

4. Conclusions

This research analysed how the metal/prepreg inter-ply friction of magnesium alloy and PA6-based FMLs varies in response to the relative sliding displacement under a wide range of normal pressures, relative sliding velocities, and temperatures typically applied in the thermoforming process of FMLs. Furthermore, the effect of the metal surface roughness was assessed. Stop-start pull-through tests with a custom-built setup were performed to evaluate the inter-ply friction coefficients. The sensitivity of the inter-ply friction in response to the different process parameters and metal surface roughness at distinct stages was determined through quantitative comparison with the experimental data. Additionally, the change from the hydrodynamic lubrication to the mixed lubrication according to the Stribeck theory was identified making use of microscopic examination of the residues on the tested magnesium alloy sheets. The main conclusions can be summarized as follows:

- When testing the FMLs at temperature higher than the melting point of the polymer matrix, the latter works as a liquid lubricant film at the interface between the metal and prepreg layers. Due to the high mobility and flow characteristics of the polymer matrix at elevated temperature, its thickness varies at varying relative sliding displacement of the plies over each other, resulting in the dynamic response of the inter-ply friction. As a result of the inter-ply friction occurring at the metal-polymer matrix interface during the first two stages under the baseline condition (T 235 °C, v 0.5 mm/s and p 2.5 MPa), the Stribeck theory classifies this condition as hydrodynamic lubrication, with a liquid-like response. The higher relative sliding displacement from the S_{w1} to the S_{w2} stage is attributed to more molten polymer matrix being evacuated from the connecting area, resulting in a thinner polymer matrix layer and further increasing the

Table 5
Fitting parameters of Eq. (12) at varying metal surface roughness.

	Sa_L			Sa_M			Sa_H		
	A	B	R^2	A	B	R^2	A	B	R^2
S_{w1}	0.047	942.30	0.9091	0.053	850.05	0.9139	0.054	866.31	0.9013
S_{w2}	0.053	863.94	0.9217	0.060	781.93	0.9121	0.061	798.70	0.9133
S_{w3}	0.058	848.43	0.9335	0.066	754.92	0.9218	0.067	780.69	0.9263
S_{w4}	0.063	812.14	0.9376	0.071	739.60	0.9405	0.073	775.19	0.9342
S_{w5}	0.067	782.98	0.9314	0.075	751.87	0.9340	0.078	787.79	0.9276

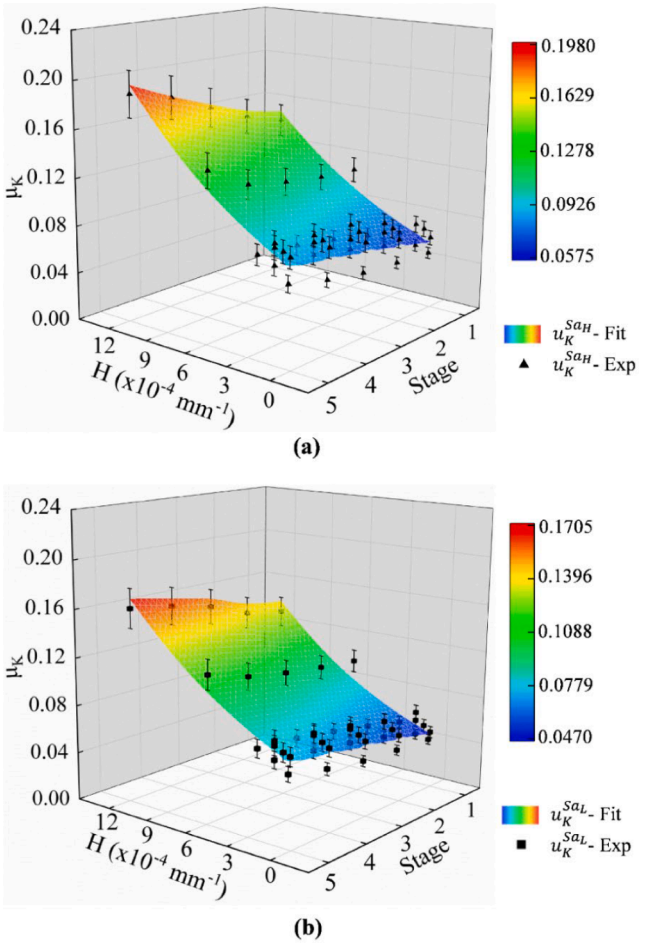

Fig. 17. Calculated and experimental kinetic inter-ply friction coefficients at varying Hersey number and stage under the metal surface roughness (a) Sa_H (b) Sa_L when the temperature is 235 °C. (For interpretation of the references to colour in this figure legend, the reader is referred to the web version of this article.)

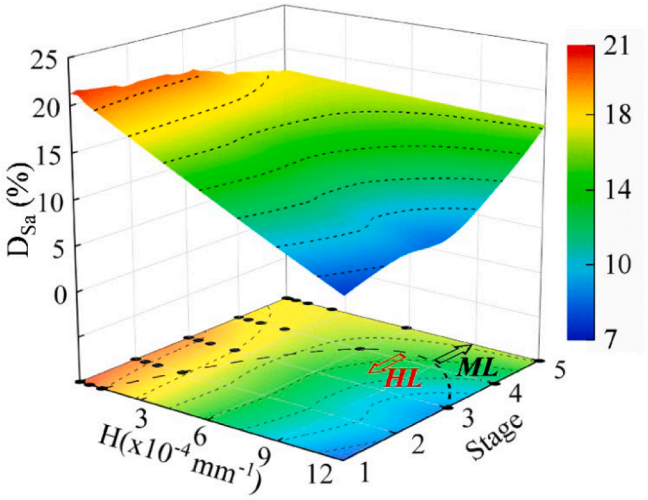

Fig. 18. Degree of the metal surface roughness influence on the variation in the kinetic friction coefficient at varying Hersey number and stage. (For interpretation of the references to colour in this figure legend, the reader is referred to the web version of this article.)

inter-ply friction coefficient. The metal surface contacts the fibre layer at the S_{w3} stage, revealing that the inter-ply friction falls into the mixed lubrication range where the response of the inter-ply friction switches to a solid-like. As the amount of contact between the metal and fibre layers increases, the inter-ply friction coefficient increases as well from the S_{w3} to the S_{w5} stage.

- The squeezing flow of the polymer matrix and the surface asperities of the fibre layer both exhibit considerable sensitivity to the normal pressure, which hence impacts the inter-ply friction. At the beginning stage, the inter-ply friction falls into the hydrodynamic lubrication region under normal pressures of 0.5 MPa and 2.5 MPa, with the latter inducing a lower inter-ply friction coefficient, while it facilitates the meeting between the fibre and metal layers as the relative sliding stage increases. When the applied normal pressure is 5 MPa, the inter-ply friction enters the mixed lubrication range at the S_{w1} stage, making the friction coefficient higher than that at the other pressure values.
- Due to the viscosity of the polymer matrix and its shear behaviour being related to the shear strain rate, the metal/polymer matrix inter-ply friction is also dependent on the relative sliding velocity. Passing from a velocity of 0.1 mm/s to 1 mm/s contributes to higher inter-ply friction and accelerates the transition from the hydrodynamic lubrication to the mixed one.
- The state and properties of the thermoplastic resin are highly sensitive to the forming temperature, further impacting the inter-ply friction. At temperature above the melting point of the thermoplastic polymer matrix (wet friction case), a reduced viscosity contributes to decrease the friction coefficients whatever the stage. On the contrary, the inter-ply friction shows a dry response dominated by the Coulomb friction when the testing temperature is below the polymer matrix melting limit, where the inter-ply friction is more sensitive to the relative sliding displacement compared to the wet friction case.
- Higher metal surface roughness also induces a higher inter-ply friction coefficient in both the wet and dry friction cases. The sensitivity of the inter-ply friction to the metal surface roughness varies throughout the lubrication regions, with the metal/fibre inter-ply friction in the mixed lubrication range being more sensitive than the one at the metal/polymer matrix interface in the hydrodynamic lubrication range.

CRediT authorship contribution statement

Zheng Liu: Conceptualization, Methodology, Investigation, Writing

– original draft. **Enrico Simonetto:** Methodology, Formal analysis, Data curation, Validation. **Andrea Ghiotti:** Resources, Project administration, Visualization. **Stefania Bruschi:** Conceptualization, Validation, Writing – review & editing, Supervision.

Declaration of Competing Interest

The authors declare that they have no known competing financial interests or personal relationships that could have appeared to influence the work reported in this paper.

Data availability

Data will be made available on request.

Acknowledgements

This work was supported by the European Union - NextGenerationEU (National Sustainable Mobility Center CN00000023, Italian Ministry of University and Research Decree n. 1033 - 17/06/2022, Spoke 11 - Innovative Materials & Lightweighting) and the China Scholarship Council (202008130148).

References

[1] Lange G, Carradò A, Palkowski H. Tailored sandwich structures in the focus of research. Mater Manuf Processes 2009;24(10–11):1150–4. https://doi.org/10.1080/10426910902978977.
[2] Sinmazçelik T, Avcu E, Bora MÖ, Çoban O. A review: fibre metal laminates, background, bonding types and applied test methods. Mater Des 2011;32(7):3671–85. https://doi.org/10.1016/j.matdes.2011.03.011.
[3] Lebaupin Y, Friedli J, Caglar B, Piccand M, Pasquier R, Michaud V. Crushing and intrusion resistance improvement of aluminum beams by carbon/epoxy composite patches. Compos Struct 2019;226:111235. https://doi.org/10.1016/j.compstruct.2019.111235.
[4] Lawcock G, Ye L, Mai YW, Sun CT. The effect of adhesive bonding between aluminum and composite prepreg on the mechanical properties of carbon-fiber reinforced metal laminates. Compos Sci Technol 1997;57:35–45. https://doi.org/10.1016/S0266-3538(96)00107-8.
[5] Takamatsu T, Matsumura T, Ogura N, Shimokawa T, Kakuta Y. Fatigue crack growth properties of a GLARE3-5/4 fiber/metal laminate. Eng Fract Mech 1999;63:253–72. https://doi.org/10.1016/S0013-7944(99)00021-1.
[6] Chai GB, Manikandan P. Low velocity impact response of fibre-metal laminates - a review. Compos Struct 2014;107:363–81. https://doi.org/10.1016/j.compstruct.2013.08.003.
[7] Pärnänen T, Alderliesten R, Rans C, Brander T, Saarela O. Applicability of AZ31B-H24 magnesium in Fibre Metal Laminates – An experimental impact research. Compos A 2012;43(1578–1586). https://doi.org/10.1016/j.compositesa.2012.04.008.
[8] Múgica JI, Aretxabaleta L, Ulacia I, Aurrekoetxea J. Impact characterization of thermoformable fibre metal laminates of 2024–T3 aluminium and AZ31B-H24 magnesium based on self-reinforced polypropylene. Compos A 2014;61:67–75. https://doi.org/10.1016/j.compositesa.2014.02.011.
[9] He W, Wang L, Liu H, Wang C, Yao L, Li Q, Sun G. On impact behavior of fiber metal laminate (FML) structures: A state-of-the-art review Thin-Walled Structures 2021 167:108026. https://doi.org/10.1016/j.tws.2021.108026.
[10] Alderliesten R, Rans C, Benedictus R. The applicability of magnesium based Fibre Metal Laminates in aerospace structures. Compos Sci Technol 2008;68:2983–93. https://doi.org/10.1016/j.compscitech.2008.06.017.
[11] Zhang X, Ma Q, Dai Y, Hu F, Liu G, Xu Z. Effects of surface treatments and bonding types on the interfacial behavior of fiber metal laminate based on magnesium alloy. Appl Surf Sci 2018;427:897–906. https://doi.org/10.1016/j.apsusc.2017.09.024.
[12] Tang H, Han Y, Wu T, Tao W, Jian X, Wu Y. Synthesis and properties of hydroxyapatite-containing coating on AZ31 magnesium alloy by micro-arc oxidation. Appl Surf Sci 2017;400:391–404. https://doi.org/10.1016/j.apsusc.2016.12.216.
[13] Hou M. Stamp forming of continuous glass fibre reinforced polypropylene. Compos Appl Sci Manuf 1997;28:695–702. https://doi.org/10.1016/S1359-835X(97)00013-4.
[14] Chen H, Li S, Wang J, Ding A. A focused review on the thermo-stamping process and simulation progresses of continuous fibre reinforced thermoplastic composites. Compos Part B Eng 2021;224:109196. https://doi.org/10.1016/j.compositesb.2021.109196.
[15] Farnand K, Zobeiry N, Poursartip A, Fernlund G. Micro-level mechanisms of fiber waviness and wrinkling during hot drape forming of unidirectional prepreg composites. Compos A Appl Sci Manuf 2017;103:168–77. https://doi.org/10.1016/j.compositesa.2017.10.008.
[16] Harrison P, Gomes R, Curado-correia N. Press forming a 0 / 90 cross-ply advanced thermoplastic composite using the double-dome benchmark geometry. Compos Part A 2013;54:56–69. https://doi.org/10.1016/j.compositesa.2013.06.014.
[17] Ten Thije R, Akkerman R, Ubbink M, Van der Meer L. A lubrication approach to friction in thermoplastic composites forming processes. Compos Part A: Appl Sci Manuf 2011;42(8):950–60. https://doi.org/10.1016/j.compositesa.2011.03.023.
[18] Chen Q, Boisse P, Park CH, Saouab A, Bréard J. Intra/inter-ply shear behaviors of continuous fiber reinforced thermoplastic composites in thermoforming processes. Compos Struct 2011;93(7):1692–703. https://doi.org/10.1016/j.compstruct.2011.01.002.
[19] Larberg YR, Åkermo M. On the interply friction of different generations of carbon / epoxy prepreg systems. Compos Part A 2011;42:1067–74. https://doi.org/10.1016/j.compositesa.2011.04.010.
[20] Fetfatsidis KA, Gamache LM, Gorczyca JL, Sherwood JA, Jauffrès D, Chen J. Design of an apparatus for measuring tool/fabric and fabric/fabric friction of woven-fabric composites during the thermostamping process. Int J Mater Form 2013;6(1):1–11. https://doi.org/10.1007/s12289-011-1058-3.
[21] Sachs U, Akkerman R, Fetfatsidis K, Vidal-Sallé E, Schumacher J, Ziegmann G, et al. Characterization of the dynamic friction of woven fabrics: Experimental methods and benchmark results. Compos Part A Appl Sci Manuf 2014;67:289–98. https://doi.org/10.1016/j.compositesa.2014.08.026.
[22] Erland S. Characterisation of uncured carbon fibre composites. University of Bath; 2016.
[23] Scherer R, Friedrich K. Inter-and intraply-slip flow processes during thermoforming of CF/PP-laminates. Compos Manuf 1991;2(2):92–6. https://doi.org/10.1016/0956-7143(91)90185-J.
[24] Chow S. Frictional Interaction Between Blank Holder and Fabric in Stamping of Woven Thermoplastic Composites. University of Massachusetts Lowell;2002.
[25] Vanclooster K, Lomov S V, Verpoest I. SIMULATION OF MULTI-LAYERED COMPOSITES FORMING. Int J Mater Form 2010; 3:695–8. https://doi.org/10.1007/s12289-010-0865-2.
[26] Kim J, Hwang Y, Baek J, Song W, Kim H. Study on inter-ply friction between woven and unidirectional prepregs and its effect on the composite forming process. Compos Struct 2021;267:113888. https://doi.org/10.1016/j.compstruct.2021.113888.
[27] Rashidi A, Montazerian H, Yesilcimen K, Milani AS. Experimental characterization of the inter-ply shear behavior of dry and prepreg woven fabrics : Significance of mixed lubrication mode during thermoset composites processing. Compos Part A 2020;129:105725. https://doi.org/10.1016/j.compositesa.2019.105725.
[28] Rashidi A, Crawford B, Olfatbakhsh T, Milani AS. A mixed lubrication model for inter-ply friction behaviour of uncured fabric prepregs. Compos Part A 2021;149:106571. https://doi.org/10.1016/j.compositesa.2021.106571.
[29] Liu S, Sinke J, Dransfeld C. An inter-ply friction model for thermoset based fibre metal laminate in a hot-pressing process. Compos Part B 2021;227:109400. https://doi.org/10.1016/j.compositesb.2021.109400.
[30] Erland S, Dodwell TJ, Butler R. Characterisation of inter-ply shear in uncured carbon fibre prepreg. Compos Part A 2015;77:210–8. https://doi.org/10.1016/j.compositesa.2015.07.008.
[31] Kim DH, Choi DH, Kim HS. Design optimization of a carbon fiber reinforced composite automotive lower arm. Compos B Eng 2014;58:400–7. https://doi.org/10.1016/j.compositesb.2013.10.067.
[32] Zhu G, Wang Z, Cheng A, Li G. Design optimisation of composite bumper beam with variable cross-sections for automotive vehicle. Int J Crashworthiness 2017;22:365–76. https://doi.org/10.1080/13588265.2016.1267552.
[33] El-Dessouky HM, Lawrence CA. Ultra-lightweight carbon fibre/thermoplastic composite material using spread tow technology. Compos B Eng 2013;50:91–7. https://doi.org/10.1016/J.COMPOSITESB.2013.01.026.
[34] Grove S, Short D. Fabrication processes for continuous fibre reinforced thermoplastics. In: The 15 th reinforced plastics congress; 1986. p. 29–31.
[35] Muflikhun MA, Higuchi R, Yokozeki T, Aoki T. Delamination behavior and energy release rate evaluation of CFRP/SPCC hybrid laminates under ENF test: Corrected with residual thermal stresses. Compos Struct 2020;236:111890. https://doi.org/10.1016/j.compstruct.2020.111890.
[36] Askari M, Javadi M, Eslami-Farsani R, Geranmayeh A. The effect of thermal and cryogenic environments on the impact performance of aluminum-glass fibers/epoxy laminated composites. Proc Inst Mech Eng C J Mech Eng Sci 2023:563–79. https://doi.org/10.1177/09544062231159485.
[37] Azghan MA, Bahari-Sambran F, Eslami-Farsani R. Modeling and experimental study on the mechanical behavior of glass/basalt fiber metal laminates after thermal cycling. Int J Damage Mech 2021;30(8):1192–212. https://doi.org/10.1177/1056789521998731.
[38] Liu J, Chaudhury MK, Berry DH, Seebergh JE, Osborne JH, Blohowiak KY. Effect of surface morphology on crack growth at a sol-gel reinforced epoxy/aluminum interface. J Adhesion 2006;82(5):487–516. https://doi.org/10.1080/00218460600713725.
[39] Prolongo S, Ureña A. Effect of surface pre-treatment on the adhesive strength of epoxy–aluminium joints. Int J Adhes Adhes 2009;29(1):23–31. https://doi.org/10.1016/j.ijadhadh.2008.01.001.
[40] Chai GB, Manikandan P. Low velocity impact response of fibre-metal laminates–a review. Compos Struct 2014;107:363–81. https://doi.org/10.1016/j.compstruct.2013.08.003.
[41] Burianek DA, Spearing SM. Fatigue damage in titanium-graphite hybrid laminates. Compos Sci Technol 2002;62(5):607–17. https://doi.org/10.1016/S0266-3538(02)00027-1.
[42] Eslami-Farsani R, Aghamohammadi H, Khalili SMR, Ebrahimnezhad-Khaljiri H, Jalali H. Recent trend in developing advanced fiber metal laminates reinforced

with nanoparticles: a review study. Journal of Industrial Textiles 2022; 51:7374S-7408S. https://doi.org/10.1177/1528083720947106.
[43] Kim Y-W. Surface modification of Ti dental implants by grit-blasting and micro-arc oxidation. Mater Manuf Proces 2010;25(5):307–10. https://www.tandfonline.com/doi/abs/10.1080/10426911003747915.
[44] Rider AN, Arnott DR. Boiling water and silane pre-treatment of aluminium alloys for durable adhesive bonding. Int J Adhes Adhes 2000;20:209–20. https://doi.org/10.1016/S0143-7496(99)00046-9.
[45] Critchlow GW, Yendall KA, Bahrani D, Quinn A, Andrews F. Strategies for the replacement of chromic acid anodising for the structural bonding of aluminium alloys. Int J Adhes Adhes 2006;26:419–53. https://doi.org/10.1016/j.ijadhadh.2005.07.001.
[46] Man H, Zhao N, Cui Z. Surface morphology of a laser surface nitrided and etched Ti–6Al–4V alloy. Surf Coat Technol 2005;192(2–3):341–6. https://doi.org/10.1016/j.surfcoat.2004.07.076.
[47] Sang Park SY, Choi WJ, Choi HS, Kwon H, Kim SH. Effects of surface pretreatment and void content on GLARE laminate process characteristics. J Mater Process Technol 2010;210:1008–16. https://doi.org/10.1016/j.jmatprotec.2010.01.017.
[48] Carradó A. Structural, microstructural, and residual stress investigations of plasma-sprayed hydroxyapatite on Ti-6Al-4 V. ACS Appl Mater Interfaces 2010;2(2):561–5. https://doi.org/10.1021/am900763j.
[49] Bachchhav B, Bagchi H. Effect of surface roughness on friction and lubrication regimes. Mater Today Proc 2020;38:169–73. https://doi.org/10.1016/j.matpr.2020.06.252.
[50] Liu Z, Simonetto E, Ghiotti A, Bruschi S. Experimental and numerical investigation of the effect of metal surface treatments on the delamination behaviour of magnesium alloy-based Fibre Metal Laminates. CIRP J Manuf Sci Technol 2022;38:442–56. https://doi.org/10.1016/j.cirpj.2022.05.015.
[51] ASTM D 1894-14. Standard test method for static and kinetic coefficients of friction of plastic film and sheeting. Annu. B. ASTM Standard International.
[52] Tadmor Z, Gogos CG. Principles of polymer processing. second ed. New York: Wiley Interscience; 2006. p. 887–911.
[53] Belnoue JPH, Nixon-Pearson OJ, Ivanov D, Hallett SR. A novel hyper-viscoelastic model for consolidation of toughened prepregs under processing conditions. Mech Mater 2016;97:118–34. https://doi.org/10.1016/j.mechmat.2016.02.019.